Research article JHEP|Reports

Oxytocin alleviates liver fibrosis via hepatic macrophages

Authors

Xiangyu Zhai, Hao Zhang, Zhijia Xia, Mingkun Liu, Gang Du, Zhengchen Jiang, Huaxin Zhou, Dan Luo, Dandan Dou, Jingxin Li, Wei Wang, Xiaosong Li, Bin Jin

Correspondence

jinglewei@sdu.edu.cn (W. Wang), lixiaosong@cqmu.edu.cn (X. Li), jinbin@sdu.edu.cn (B. Jin).

Graphical abstract

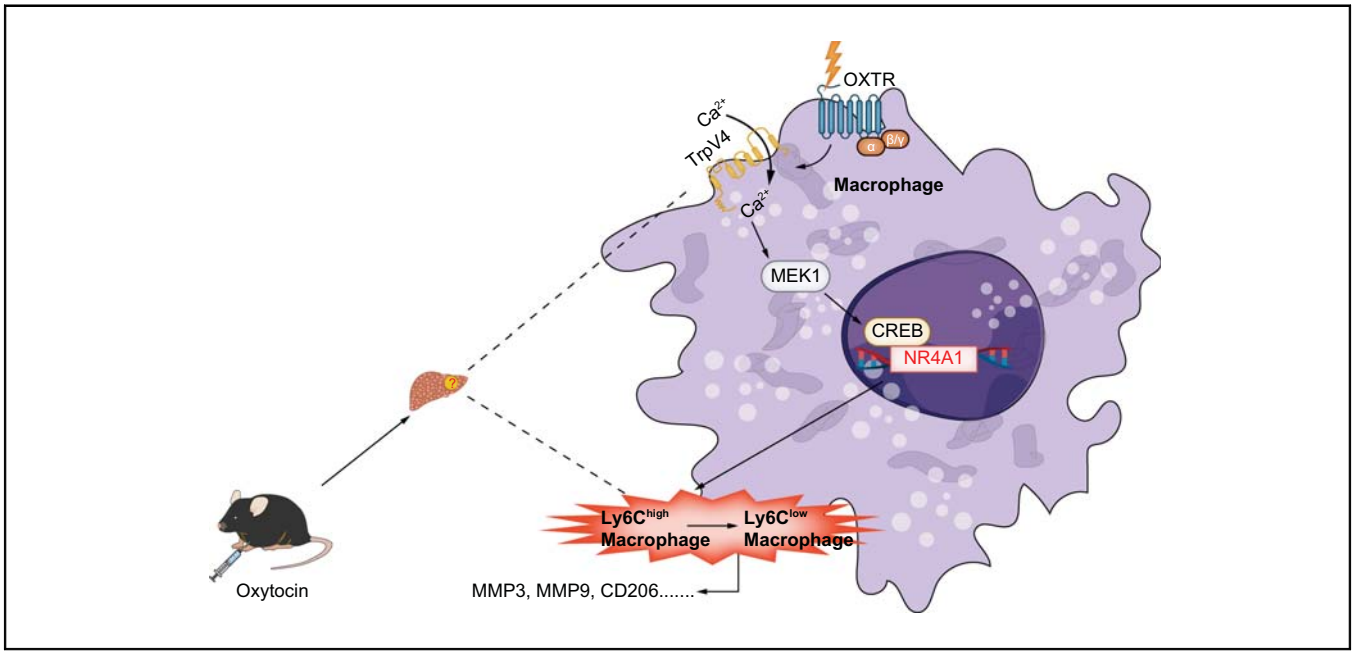

Highlights

- This study marks the first discovery of the therapeutic role of oxytocin in hepatic fibrosis.
- Single-cell sequencing identifies oxytocin target cells.
- Alteration of Ly6C^{high}/Ly6C^{low} phenotype by oxytocin has been observed.
- Oxytocin achieves Nr4a1 activation by promoting intracellular flow of calcium ions.

Impact and implications

Previous studies revealed for the first time the expression of oxytocin receptors in the liver. The present study shows that oxytocin reverses hepatic fibrosis and that hepatic macrophages are the central hub of oxytocin-mediated alleviation of hepatic fibrosis by promoting a phenotypic switch in hepatic macrophages, transitioning from Ly6^{high} to Ly6C^{low} expression. The present study reveals a novel pathway by which oxytocin regulates macrophage phenotype. In addition, the potential applications of oxytocin and its analogues, as traditional drugs for clinical application, in the treatment of liver fibrosis deserve to be further explored.

https://doi.org/10.1016/j.jhepr.2024.101032

Research article

JHEP|Reports

Oxytocin alleviates liver fibrosis via hepatic macrophages

Xiangyu Zhai,[1,2,†] **Hao Zhang**,[1,2,†] **Zhijia Xia**,[3,†] Mingkun Liu,[4] Gang Du,[2,4] Zhengchen Jiang,[2,5] Huaxin Zhou,[1,2] Dan Luo,[6] Dandan Dou,[7] Jingxin Li,[7] Wei Wang,[8,*] Xiaosong Li,[9,*] Bin Jin[1,2,4,*]

[1]*Department of Hepatobiliary Surgery, The Second Hospital of Shangdong University, Jinan, China;* [2]*Hepatobiliary Surgery Research Center of Shandong University, Jinan, China;* [3]*Department of General, Visceral and Transplantation Surgery, University of Heidelberg, Heidelberg, Germany;* [4]*Organ Transplant Department, Qilu Hospital of Shangdong University, Jinan, China;* [5]*Department of General Surgery, Shandong Provincial Qianfoshan Hospital, Cheeloo College of Medicine, Shandong University, Jinan, China;* [6]*Pathology Tissue Bank, Qilu Hospital of Shandong University, Jinan, China;* [7]*Department of Physiology, School of Basic Medical Sciences, Cheeloo College of Medicine, Shandong University, Jinan, China;* [8]*Medical Integration and Practice Center, Shandong University, Jinan, China;* [9]*Clinical Molecular Medicine Testing Center, The First Affiliated Hospital of Chongqing Medical University, Chongqing, China*

JHEP Reports **2024.** https://doi.org/10.1016/j.jhepr.2024.101032

Background & Aims: Previous studies demonstrated oxytocin treatment effectiveness in reducing mortality and reversing liver fibrosis in mice. However, the underlying mechanism remains obscure, given the absence of oxytocin receptor expression in hepatic stellate cells, the primary liver fibrosis effector cells.

Methods: A comprehensive map of cell populations in fibrotic liver was generated using single-cell sequencing. The map enabled our study of the target cells of oxytocin action in the liver in more dimensions. Furthermore, we elucidated the mechanism of the oxytocin signaling system in hepatic macrophages using oxytocin receptor-specific knockout mice and liver fibrosis animal models.

Results: The carbon tetrachloride-induced hepatic fibrosis and bile duct ligation hepatic fibrosis mouse models demonstrated that oxytocin reversed hepatic fibrosis in mice. The mapped liver cell populations demonstrated that oxytocin promoted the phenotypic switch from $Ly6^{high}$ to $Ly6C^{low}$ in myeloid-derived macrophages. The phenotypic control of oxytocin signaling system activation on this phenotypic switch was validated using myeloid-specific oxytocin receptor knockout mice. Subsequent studies demonstrated that the calcium inward flow induced by oxytocin receptor activation activated the key orphan nuclear receptor NR4A1, which controls macrophage phenotypic switching. Specifically, calcium ions activated CREB, a key target regulator of NR4A1 expression.

Conclusions: The findings established hepatic macrophages as a hub responsible for the oxytocin-mediated alleviation of liver fibrosis. This study revealed a novel pathway where oxytocin regulates macrophage phenotype.

Impact and implications: Previous studies revealed for the first time the expression of oxytocin receptors in the liver. The present study shows that oxytocin reverses hepatic fibrosis and that hepatic macrophages are the central hub of oxytocin-mediated alleviation of hepatic fibrosis by promoting a phenotypic switch in hepatic macrophages, transitioning from $Ly6^{high}$ to $Ly6C^{low}$ expression. The present study reveals a novel pathway by which oxytocin regulates macrophage phenotype. In addition, the potential applications of oxytocin and its analogues, as traditional drugs for clinical application, in the treatment of liver fibrosis deserve to be further explored.

Introduction

Oxytocin is the first neuropeptide to be sequenced and synthesized[1] and exhibits a wide range of functions and therapeutic benefits in conditions such as autism spectrum disorder,[2] post-traumatic stress disorder,[3] pain management,[4] and malignant tumors.[5] Accordingly, oxytocin has gained recognition as a natural medicinal agent.[6]

Previously, we demonstrated the presence of oxytocin receptors (OXTRs) in the liver and revealed the potential of exogenous oxytocin to promote hepatocyte proliferation in aged mice by inducing autophagy.[7] Our findings suggested that exogenous oxytocin significantly prolonged mouse survival and alleviated hepatic fibrosis in a carbon tetrachloride (CCl_4)-induced liver injury model. However, our previous publication did not explicitly address these specific findings. Interestingly, despite hepatic stellate cells (HSCs) being the primary effector cells of extracellular matrix (ECM) production in liver fibrosis, they do not express OXTRs.[7] This finding raises questions about the liver fibrosis reversal mechanisms. Although previous studies have suggested the involvement of various liver cell types in attenuating fibrosis,

Keywords: Oxytocin; Liver fibrosis; Hepatic macrophages; NR4A1.

Received 9 May 2023; received in revised form 22 January 2024; accepted 26 January 2024; available online 5 February 2024

† These authors contributed equally to this work.

* Corresponding authors. Addresses: Medical Integration and Practice Center, Shandong University, Jinan 250012, China (W. Wang); Clinical Molecular Medicine Testing Center, The First Affiliated Hospital of Chongqing Medical University, Chongqing 400016, China (X. Li); Department of Hepatobiliary Surgery, The Second Hospital of Shangdong University, Beiyuan Road No. 247, Jinan 250033, China. Tel.: +86-15098772066 (B. Jin).

E-mail addresses: jinglewei@sdu.edu.cn (W. Wang), lixiaosong@cqmu.edu.cn (X. Li), jinbin@sdu.edu.cn (B. Jin).

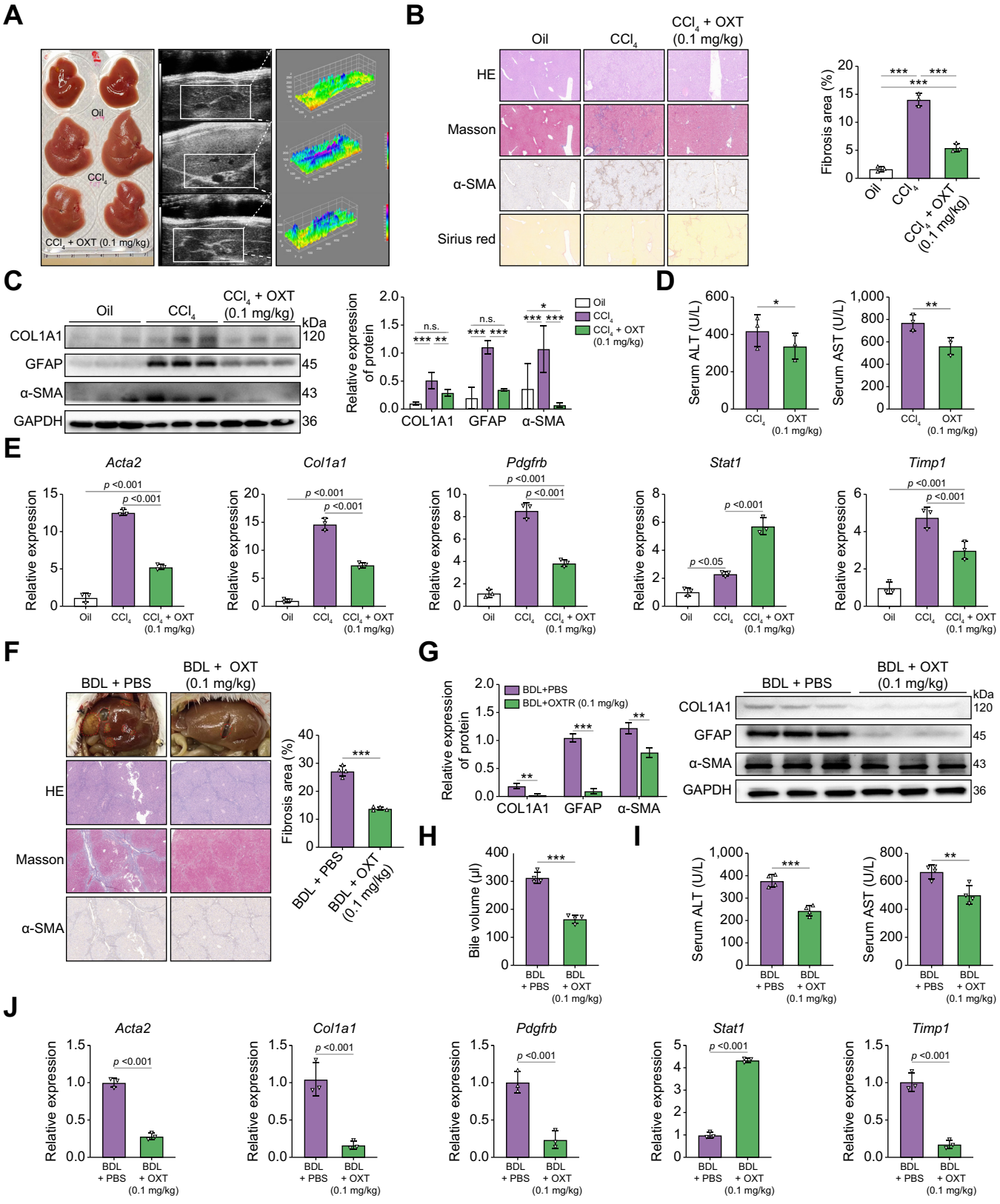

Fig. 1. OXT alleviates liver fibrosis *in vivo*. (A) Representative *in vivo* ultrasound imaging of the hepatoportal region of the liver in different groups of mice 6 weeks after CCl_4 injection. The increase in liver echo intensity and heterogeneity demonstrated the development of hepatic fibrosis. The severity of hepatic fibrosis was analyzed using integrated echo intensity (image brightness). (B) Representative immunohistochemical staining of Sirius Red, α-SMA, and Masson's trichrome in CCl_4-induced fibrotic livers from three different groups: oil, CCl_4, and OXT-treated. The percentage of α-SMA-positive cells was quantified and averaged using ImageJ v1.4 in five randomly selected regions of each mouse separately (n = 3 biologically independent mice per group). Scale bars: 100 μm. (C)

an understanding of the precise mechanism of liver fibrosis reversal by oxytocin remains incomplete. Accordingly, we investigated and elucidated the intricate mechanisms underlying the oxytocin-mediated reversal of liver fibrosis via genetic mouse models and single-cell sequencing technology.

Materials and methods

Mice and treatments

Male C57BL/6 mice (8 weeks old) were from the Shandong University Experimental Animal Center. The OXTR floxed ($OXTR^{FL/FL}$) mice (stock no. 008471) and LysM-Cre transgenic mice (stock no. 004781) were from Jackson Laboratory. The Alb-Cre mice were kindly donated by Prof. Jingxin Li. The $OXTR^{FL/FL}$ mice were crossed with the LysM-Cre transgenic mice to generate myeloid-specific OXTR knockout mice ($OXTR^{myel\text{-}KO}$), and their $OXTR^{FL/FL}$ litter mates were used as the myeloid-specific OXTR wild-type (WT) control ($OXTR^{myel\text{-}WT}$). Furthermore, the $OXTR^{FL/FL}$ mice were crossed with the Alb-Cre transgenic mice to generate hepatocyte-specific OXTR knockout mice ($OXTR^{fl/fl,\ alb\text{-}cre}$), and their $OXTR^{FL/FL}$ litter mates were used as the WT control. All mice were kept in a sterile environment at 25 °C, 50% air humidity, and a 12-h/12-h light/dark cycle. All animal studies were performed in accordance with the ethics code approved by the Shandong University Ethics Committee.

The CCl_4-induced liver fibrosis model was established by injecting mice i.p. with 1 μl/g CCl_4/olive oil (1/7, v/v) twice weekly. The oxytocin treatment and control groups were i.p. injected with 0.1 mg/kg oxytocin and PBS every 2 days, respectively. The serum aspartate aminotransferase (AST) and alanine aminotransferase (ALT) levels were detected 48 h after the CCl_4 injection.

The hepatic fibrosis model of bile duct ligation (BDL) and cholestasis was established by ligating the mouse common bile duct with a 4-0 suture for 4 weeks to complete the establishment of the liver fibrosis model. The mice received i.p. injections of 0.1 mg/kg oxytocin (sterile PBS as solvent) every 2 days.

Mice displaying severe discomfort (ascites, reduced mobility, and overall malaise) were used as a humane endpoint. These mice were anesthetized with 2% isoflurane and then euthanized humanely by rapid cervical dislocation.

Clinical specimens

Liver tissue was obtained from volunteer patients who had undergone hepatic hemangioma removal at the Second Hospital of Shandong University. This study was performed in accordance with the ethics code approved by the Shandong University Ethics Committee.

Ultrasound imaging

The mouse liver fibrosis development was monitored using a VisualSonics (Vevo LAZR, Canada) ultrasound imaging system. The mice were anesthetized with 2% isoflurane and then placed in the supine position on a processing table equipped with heat preservation function. Their electrocardiograph was obtained. The abdominal fur was removed using a depilatory agent, and the substernal liver area was scanned after ultrasound transmission gel had been applied. The liver was imaged in the parasternal long-axis view. Three measurements were obtained in the portal vein area. The brightness of each echohepatograph was quantified by integrated density using ImageJ v1.4.

Immunofluorescence and histological staining

The liver specimens were rinsed with PBS and fixed in 4% paraformaldehyde overnight at 4 °C. Subsequently, the specimens were dehydrated with 15 and 30% sucrose solution overnight at 4 °C. Then, the tissues were snap-frozen in O.C.T. (SAKURA Tissue-Tek). The frozen sections were osmotically treated and blocked with 5% goat serum for 1 h at room temperature. Then, the specimens were incubated overnight with the primary antibody at 4 °C and subsequently with the fluorescent secondary antibody at 37 °C for 1 h. Finally, the plates were mounted using DAPI. All paraffin-embedded tissues were excised, rinsed with PBS, and fixed in 4% paraformaldehyde for 48 h at 4 °C. Next, the tissues were rinsed with water and immersed in 70% ethanol solution until paraffin-embedded. The specimens then underwent immunofluorescence and histological staining, as previously described.[8,9] The fluorescence staining (ZSBG-BIO, China), immunohistochemical staining (ZSGB-BIO), Masson trichrome staining (Abcam, USA), and immunofluorescence and immunohistochemical image scanning were performed according to the manufacturer's protocols (3DHISTECH, Pannoramic MIDI, Pannoramic 250 Flash). Positive signals were quantified using ImageJ v1.4.

Western blotting

Proteins were extracted with 0.5% SDS and quantified using a bicinchoninic acid protein quantification kit (Beyotime, China). Polyvinylidene fluoride membranes were incubated overnight at 4 °C with primary antibodies and then for 1 h with the corresponding secondary antibodies at room temperature. Immunoreactive bands were colored using an ECL detection kit (Beyotime) and imaged using a chemiluminescence series image capture system (Thermo Fisher Scientific, USA).

The co-immunoprecipitation (co-IP) assay was performed using a Pierce Crosslink Magnetic IP/Co-IP Kit (Thermo Fisher Scientific) according to the manufacturer's instructions. Whole-cell lysates were incubated with the desired antibodies, and

COL1A1, α-SMA, and GFAP protein expressions in CCl_4-induced fibrotic livers from the oil, CCl_4, and OXT-treated groups. (D) Serum ALT and AST liver injury profiles of mice from the CCl_4 and OXT-treated groups at Week 6 after CCl_4 injection (n = 3 biologically independent mice per group). (E) Expression of *Acta2, Col1a1, Pdgfrb, Stat1*, and *Timp1* in fibrotic livers of the control and OXT-treated groups. (F) Representative immunohistochemical staining for H&E, α-SMA, and Masson's trichrome in bile-duct-ligated cholestatic fibrotic livers of the control and OXT-treated groups. The mean percentage of α-SMA-positive cells was quantified and averaged using Image =J v1.4 in five randomly selected regions of each mouse separately (n = 3 biologically independent mice per group). Scale bars: 100 μm. (G) COL1A1, α-SMA, and GFAP protein expressions in fibrotic livers of the control and OXT-treated groups. (H) Content of bile in the gallbladder of mice in the control and OXT-treated groups after BDL. (I) Serum ALT and AST liver injury profiles of mice in each group at Week 4 (n = 4 biologically independent mice per group). (J) Expression of *Acta2, Col1a1, Pdgfrb, Stat1*, and *Timp1* in fibrotic livers of the control and OXT-treated groups. Statistical analyses were performed using a two-tailed unpaired *t* test or one-way ANOVA with Tukey's *post hoc* test. Error bars indicate SEM; **p* <0.05, ***p* <0.01, ****p* <0.001, *****p* <0.0001. α-SMA, α-smooth muscle actin; ALT, alanine aminotransferase; AST, aspartate aminotransferase; BDL, bile duct ligation; CCl_4, carbon tetrachloride; GAPDH, glyceraldehyde phosphate dehydrogenase; GFAP, glial fibrillary acidic protein; OXT, oxytocin.

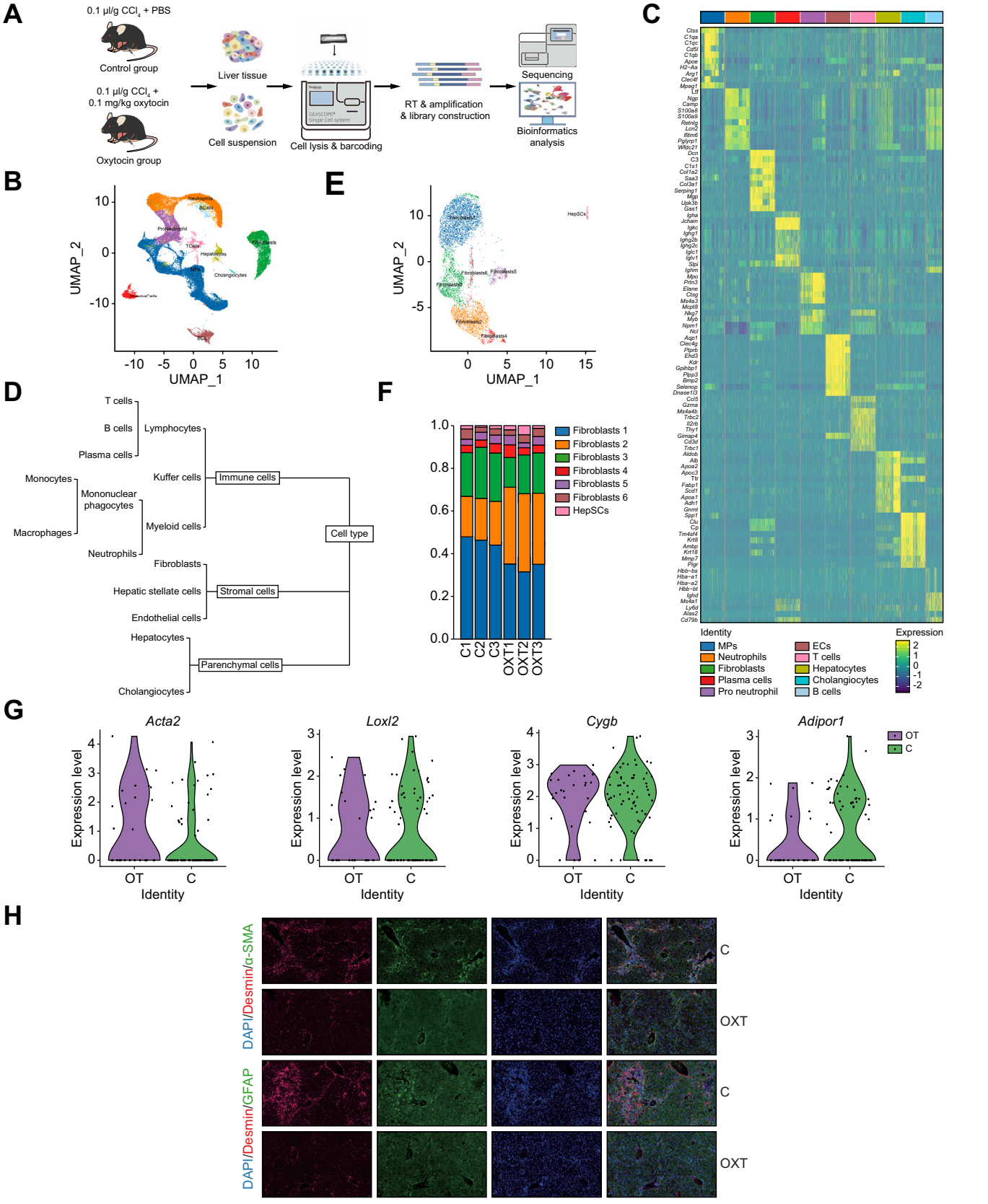

Fig. 2. Single-cell atlas of liver from the control and OXT-treated groups. (A) Schematic diagram of the experimental flow of single-cell sequencing. (B and C) The UMAP plot of 52,162 high-quality cells to visualize cell-type clusters based on the expression of known marker genes. (D) Classification of cell types based on the expression of known marker genes. (E) UMAP analysis of 6,207 fibroblasts from the control and OXT-treated group livers identified six distinct clusters of fibroblasts (1–6). (F) The relative percentage of different distinct clusters of fibroblasts for each group. (G) Violin plots showing the expression levels of different fibroblast activation marker genes across the control and OXT-treated group. (H) Fluorescent double labelling of hepatic stellate cell marker proteins and activator proteins using Desmin (red), GFAP (green), and α-SMA (green) probes. Scale bars: 50 μm. α-SMA, α-smooth muscle actin; EC, endothelial cells; GFAP, glial fibrillary acidic protein; MP, mononuclear phagocytes; OXT, oxytocin; RT, reverse transcription; UMAP, uniform manifold approximation and projection.

then the target proteins were pulled down using protein A/G magnetic beads. The microbeads were washed with a lower concentration of binding buffer to separate the binding protein from the antibody-bound microbeads. The eluate was collected and assayed using Western blotting and SDS-PAGE. The Western blotting and co-IP assays were performed, as described previously.[10]

RNA extraction and qRT-PCR

Total RNA was extracted using TRIzol (Invitrogen, USA). The quantitative real-time PCR (qRT-PCR) was performed according to ChamQ Universal SYBR qPCR Master Mix instructions (Vazyme, Nanjing, China).[10]

Cell culture

The rat HSC-T6, mouse macrophage (Raw264.7), murine skin fibroblast (L929), and human monocyte (THP-1) cell lines were from Procell Life Science & Technology. All cell lines tested negative for mycoplasma contamination. The HSC-T6, L929, and Raw264.7 cells were cultured in high-sugar DMEM (Gibco), 10% FBS (Gibco), and 1% antibiotic–antifungal (Gibco) additives at 37 °C and 5% humidity. The THP-1 cells were cultured in a completely supplemented RPMI 1640 cell culture medium (Gibco) containing 10% heat-inactivated FBS, 1% antibiotic–antifungal (Gibco), and 0.05 nM 2-mercaptoethanol. Bone marrow-derived macrophages (BMDMs) were collected from adult C57BL/6 male mice and prepared according to established protocols. The bone marrow-derived cells were differentiated into BMDMs after 7 days of culture in a humidified environment at 37 °C with 5% CO_2. The BMDMs were polarized using 100 ng/ml lipopolysaccharide (LPS) (Solabio) in DMEM for 24 h. Pro-inflammatory Raw264.7 cells were obtained after a 24-h differentiation in a medium containing 400 ng/ml LPS. The THP-1 monocytes were differentiated into macrophages via a 24-h incubation with 100 ng/ml phospho-12-myristate-13-acetate in RPMI 1640 medium, followed by a 24-h rest in fresh RPMI 1640 medium. The macrophages were stimulated with 100 ng/ml LPS to polarize them to a pro-inflammatory phenotype. Activated HSC-T6 cells were obtained after a 24-h stimulation using 10 ng/ml transforming growth factor-beta (TGF-β) (Solabio).

Mouse BMDM isolation

Bone marrow was flushed from the mouse femurs and tibiae using 5 ml precooled PBS containing 2% FBS. Solid debris was removed from the bone marrow suspension by filtering through a 40-μm cell strainer. The bone marrow suspension was centrifuged at 450 × *g* for 10 min, and then 10 ml of erythrocyte lysis buffer was added and dissociated for 2 min. The cells were resuspended in DMEM supplemented with 10% heat-inactivated FBS, 1% antibiotic–antimycotic (Gibco), and 20% L929-conditioned medium, and distributed into 100-mm Petri dishes (3×10^6 cells per dish).

Serum preparation and quantification of AST, ALT, MMP9, and TIMP1

Whole blood was allowed to stand at room temperature for 30 min and then centrifuged at 3,000 rpm for 15 min. The serum was transferred to a 1.5-ml EP tube (stored at −80 °C). The AST or ALT levels were measured using assay kits (Nanjing Jian Cheng Bioengineering Institute) according to the manufacturer's recommendation. The matrix metalloproteinase 9 (MMP9) and tissue inhibitor of metalloproteinase 1 (TIMP1) concentrations were measured using ELISA kits (Thermo Fisher Scientific).

Single-cell sequencing

Single-cell suspensions (2×10^5 cells/ml) in PBS (HyClone) were loaded onto a microwell chip using the Singleron Matrix® Single Cell Processing System. Barcode beads were subsequently collected from the microwell chip, followed by reverse transcription of the mRNA captured by the barcoding beads to obtain complementary DNA (cDNA) and PCR amplification. The amplified cDNA was fragmented and ligated using sequencing adapters. Single-cell RNA sequencing libraries were constructed according to the GEXSCOPE® Single Cell RNA Library Kit protocol (Singleron). Individual libraries were diluted to 4 nM, pooled, and sequenced on an Illumina NovaSeq 6000 using 150-bp paired-end reads.

Flow cytometry assay

Single-cell suspensions were obtained from fresh liver tissue using a gentleMACS tissue dissociation instrument. Hepatic macrophages were isolated by density gradient centrifugation using Percoll. The collected cells were washed and diluted to 1×10^6 cells/ml with PBS. Next, a 1 ml cell suspension was centrifuged. Red blood cells were lysed, stained with multicolor antibodies, and fixed in paraformaldehyde. The cells were analyzed with the BD LSR II or LSRFortessa instruments. All data were acquired using BD FACSDIVA v8.0.1 and analyzed using FlowJo v10 (TreeStar). The FACS gating strategy for $Ly6^{high}$ and $Ly6C^{low}$ macrophages from digested liver single-cell suspension was viable CD45+Ly6G-CD11b+F4/80+$Ly6^{high}$ cells and live CD45+Ly6G-CD11b+F4/80+$Ly6C^{low}$ cells, respectively.

Calcium ion measurement

Intracellular calcium ion levels were monitored using the fluorescent indicator Fluo-4 AM. A 2 μM Fluo-4 AM calcium ion probe was added to the cells 30 min before the oxytocin and calcium ion channel blocker treatment. Real-time analysis of live cells was performed using the Nikon TiE Calcium Imaging System. Continuous fluorescence intensity values were analyzed using GraphPad.

Dual-luciferase assay

A dual-luciferase assay kit (Promega, Madison, WI, USA) was used for double luciferase assay. WT and mutant CREB were inserted into the pGl3 basic vector plasmid. Lipofectamine 3000 (Thermo Fisher Scientific) was used for transient transfection. Then, 1 or 2 days later, luciferase activity was measured using a Dual-Glo Luciferase Assay System (Promega), and the firefly luciferase activity was normalized using *Renilla* luciferase activity.

ChIP assay

A chromatin immunoprecipitation (ChIP) detection kit (Thermo Fisher Scientific) was used for ChIP detection. The sample was cross-linked with 1% formaldehyde and underwent ultrasonic treatment to obtain a 200- to 500-bp DNA fragment. Then, the ultrasound-treated samples were immunoprecipitated using 2 μg anti-CREB or anti-IgG antibody. Finally, qRT-PCR analysis was performed after the immune complexes had been eluted and crosslinks reversed.

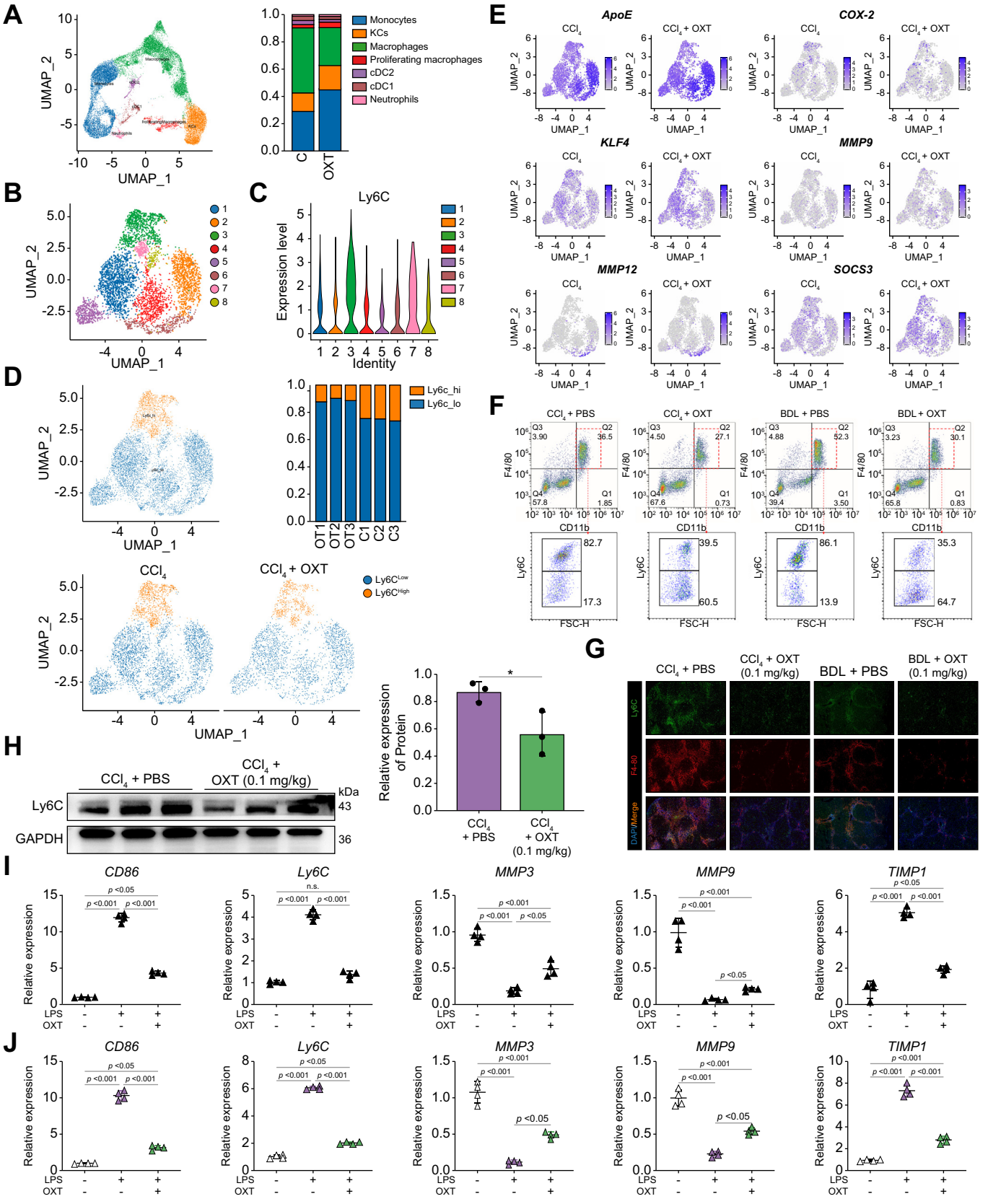

Fig. 3. OXT drives macrophage phenotype switch. (A) The UMAP plot of 20,469 high-quality cells to visualize MP clusters based on the expression of known marker genes. In the OXT-treated group, the percentage of monocyte cells within the MP cell cluster was significantly higher, whereas the percentage of monocyte-derived macrophage cells was reduced. (B) UMAP plot depicting the distribution of macrophage lineages in the atlas (n = 8 subgroups). (C) Among the eight subgroups of macrophages, the expression of Ly6C in each subgroup. (D) Macrophages were classified into Ly6C^{low} and Ly6C^{high} populations based on Ly6C

Statistical analyses

SPSS 22.0 (SPSS, Chicago, IL, USA) was used for all statistical analyses. Student's *t* test was performed to compare the two groups of data. The correlation between the variables was evaluated using Spearman's coefficient. Unless otherwise stated, all experiments were repeated three to five times independently. A *p* value of ≤0.05 was considered statistically significant.

Results

Oxytocin alleviates liver fibrosis *in vivo*

An experimental liver fibrosis model was established via a 6-week administration of CCl_4. Fibrosis progression was monitored using liver ultrasound, which assessed the reflection of ultrasound waves at the interface and changes in stiffness as brightness indicators in the ultrasound image. Oxytocin treatment was initiated 2 weeks after the CCl_4 injection once mild liver fibrosis had developed. Remarkably, oxytocin reversed the CCl_4-induced liver fibrosis, which was observed as a reduction in echo intensity around the porta hepatis, resulting in a more homogeneous appearance than that in the control group (Fig. 1A). The immunohistochemistry and Western blotting analyses revealed that oxytocin downregulated α-smooth muscle actin (α-SMA) expression and collagen deposition (a major ECM component) in the liver. In addition, the expression of glial fibrillary acidic protein (GFAP), an HSC activation indicator, was decreased. Two major enzymes (ALT and AST) are released into the bloodstream during liver injury. Oxytocin treatment significantly decreased the serum ALT and AST levels compared with the control (Fig. 1D). Furthermore, oxytocin significantly decreased the expression levels of pro-fibrotic and pro-inflammatory factors (*ACTA2*, *COL1A1*, *PDGFRB*, and *TIMP1*) while increasing the expression of the HSC activation inhibitor gene *STAT1* (Fig. 1E). Oxytocin efficacy was investigated further by expanding the study, increasing the number of mice, and extending the CCl_4 injection period to 8 weeks. Remarkably, the mice in the oxytocin treatment group had a significantly prolonged survival time compared with the control group (Fig. S1A).

In addition, an experimental cholestatic hepatic fibrosis model was established through 4-week BDL. Immunohistochemistry and Western blotting analyses demonstrated that oxytocin downregulated liver α-SMA expression and collagen deposition. Furthermore, GFAP expression was decreased (Fig. 1F and G). Moreover, the oxytocin treatment group had a significantly reduced degree of gallbladder cholestasis compared with the control group (Fig. 1H). Oxytocin also significantly decreased the serum ALT and AST levels compared with the control (Fig. 1I). Furthermore, *ACTA2*, *COL1A1*, *PDGFRB*, and *TIMP1* expression was significantly decreased, whereas *STAT1* gene expression was increased in the oxytocin group compared to the control (Fig. 1J). Notably, oxytocin definitively prolonged the survival of the cholestatic mice (Fig. S1B).

Single-cell transcriptomic atlas of liver cells

We performed single-cell sequencing of livers from three CCl_4 liver fibrosis model controls and three oxytocin-treated groups (Fig. 2A). The data indicated that 52,162 liver cells from the three control (26,930 cells) and three oxytocin-treated groups (25,232 cells) were quality-controlled to yield a high-quality single-cell transcriptome. Cluster identities were determined based on the expression of established markers after performing uniform manifold approximation and projection (UMAP) analysis (Fig. 2B and C). These cells were classified into 10 major cell lineages, each containing cells from the control and oxytocin groups: T cells, B cells, plasma cells, neutrophils, neutrophil progenitor cells, fibroblasts, endothelial cells, mononuclear phagocytes, hepatocytes, and cholangiocytes (Fig. 2D).

The role of oxytocin in liver fibrosis was investigated by focusing on liver fibroblast populations. Single-cell sequencing analysis of 6,207 fibroblasts from the control and oxytocin groups revealed six distinct subpopulations (fibroblasts 1–6; Fig. 2E). Comparison of the two groups revealed significant differences in the distribution of these subpopulations. Interestingly, the oxytocin group had an increased proportion of fibroblasts within hepatic fibroblast subpopulation 2, whereas subpopulations 1 and 3 had decreased fibroblast proportions compared with the control group (Fig. 2F). This suggested that oxytocin influenced fibroblast heterogeneity in the liver. Furthermore, our analysis revealed differential expression of pro-fibrotic marker genes in fibroblasts between the control and oxytocin groups. Oxytocin treatment was associated with reduced expression of pro-fibrotic genes, indicating its potential to mitigate fibrosis progression specifically in fibroblasts (Fig. 2G and H). These findings supported oxytocin efficacy in mitigating pro-fibrotic processes specifically within the liver fibroblast population.

Macrophages: target cells of oxytocin action in reversing hepatic fibrosis

Hepatocytes are the principal parenchymal cells in the liver and are crucial in liver fibrosis. The direct damage by CCl_4 on the liver substantially decreased the number of surviving hepatocytes and cholangiocytes compared with the other cell groups (Fig. 2B). Consequently, single-cell sequencing outcomes alone cannot accurately depict hepatocyte OXTR involvement during liver fibrosis treatment. To address this limitation, we bred mice with targeted knockout of OXTRs specifically in hepatocytes (Fig. S2A) and subsequently examined the influence of hepatocytes on fibrosis reversal via oxytocin treatment in a CCl_4-induced hepatic fibrosis model. The findings revealed that silencing the

expression of eight macrophage subpopulations. The proportion of $Ly6C^{low}$ macrophage cluster cells was increased in the OXT-treated group compared with the control group. Conversely, the percentage of $Ly6C^{high}$ macrophage cluster cells decreased in the OXT-treated group. (E) Expression of Ly6C macrophage marker genes *ApoE*, *KLF4*, *SOCS3*, *MMP9*, *MMP12*, and *COX-2* in the control group and OXT-treated group. (F) In the CCl_4-induced liver fibrosis and BDL models, the ratio of $Ly6C^{high}$ and $Ly6C^{low}$ macrophage was detected via flow cytometry. (G and H) Expression of Ly6C in the liver in two liver fibrosis models. Scale bars: 100 μm. (I and J) Relative mRNA expression levels of *Ly6C*, *CD86*, *MMP3*, *MMP9*, and *TIMP1* in LPS-stimulated BMDM/THP-1 with or without OXT treatment. Statistical analyses were performed using a two-tailed unpaired *t* test or one-way ANOVA with Tukey's *post hoc* test. Error bars indicate SEM; *p <0.05, **p <0.01, ***p <0.001, ****p <0.0001. BDL, bile duct ligation; CCl_4, carbon tetrachloride; FSC-H, forward scatter height; LPS, lipopolysaccharide; MMP3/9, matrix metalloproteinase 3/9; OXT, oxytocin; TMP1, tissue inhibitor of metalloproteinase 1; UMAP, uniform manifold approximation and projection.

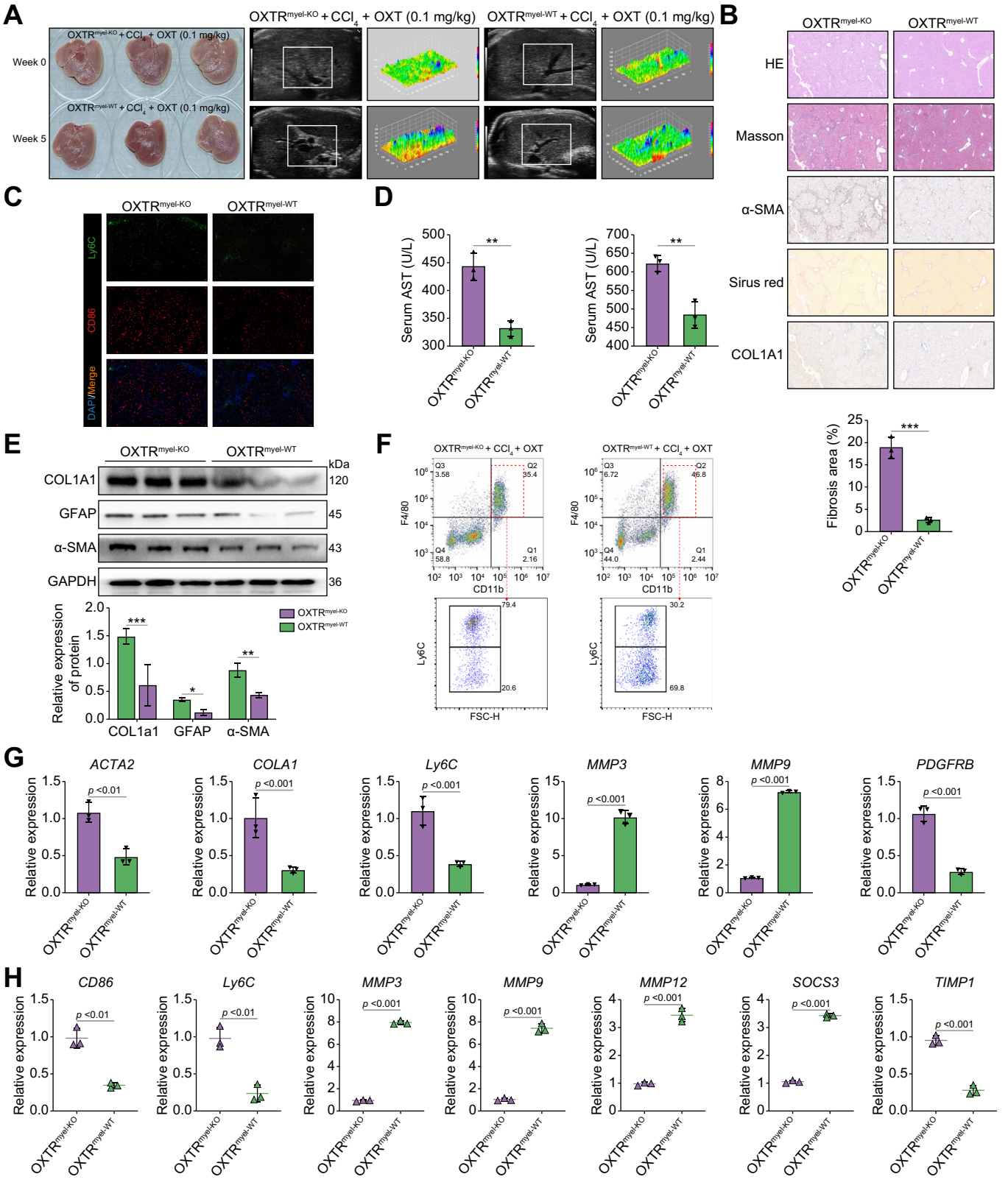

Fig. 4. OXTR knockout mice further validate the therapeutic effects of oxytocin on liver fibrosis and drive macrophage phenotype switching. (A) Representative *in vivo* ultrasound imaging of mouse livers from different groups 5 weeks after CCl_4 injection. Compared with mice in the $OXTR^{myel\text{-}WT}$ group, mice in the $OXTR^{myel\text{-}KO}$ group showed hyperechoic ultrasound in the location of typical hepatic fibrosis in the portal vein area. In addition, the degree of hepatic fibrosis in the $OXTR^{myel\text{-}KO}$ group was higher than that in the $OXTR^{myel\text{-}WT}$ group. (B) Representative immunohistochemical staining of H&E, Sirius Red, α-SMA, COL1A1, and Masson's trichrome in CCl_4-induced fibrotic livers from the $OXTR^{myel\text{-}KO}$ and $OXTR^{myel\text{-}WT}$ groups. Immunohistochemical staining showed that the degree of liver fibrosis was significantly higher in the $OXTR^{myel\text{-}KO}$ group than in the $OXTR^{myel\text{-}WT}$ group. Scale bars: 50 μm. (C) Immunofluorescence results

hepatocyte OXTR did not yield significant variations in oxytocin treatment efficacy for liver fibrosis (Fig. S2B). These results suggested that hepatocytes might not be a decisive factor in oxytocin-mediated fibrosis reversal.

Mesenchymal cell populations (fibroblasts and HSCs) are the primary effector cells driving liver fibrosis progression. Previously, we suggested the absence of OXTR expression in hepatic mesenchymal cells. Hence, it is unlikely that exogenous oxytocin directly affects mesenchymal cells to exert its therapeutic effects on liver fibrosis.[7]

Liver immune cells are important in maintaining liver homeostasis. Therefore, we re-analyzed the single-cell sequencing data. The results demonstrated no significant changes in the lymphocyte (B cells, T cells, and plasma cells) and neutrophil populations in the oxytocin group compared with the control group, and the transcriptome results demonstrated no significant genetic differences (Fig. S2C and D). Furthermore, we investigated the effects of oxytocin on OXTRs in neutrophils and lymphocytes using immunofluorescence. The results demonstrated that oxytocin did not affect OXTR expression in those cells (Fig. S2E). Therefore, the above immune cells were not pivotal in the fibrotic treatment with oxytocin.

Because of the similarity of markers and functional genes, cell populations such as monocytes, monocyte-derived macrophages, and Kupffer cells are collectively referred to as MP cell populations in Fig. 2B. Notably, the percentage of monocyte cells within the MP cell cluster in the oxytocin group was significantly higher, whereas the percentage of monocyte-derived macrophage cells was reduced (Fig. 3A). This finding aligned with our observation of the decreased expression of a chemokine family that is crucial in recruiting hepatic macrophages (Fig. 6B). The nine clusters formed by monocytes demonstrated no notable differences in the proportion of each cluster between the control and oxytocin groups (Fig. S3A and B). Furthermore, the groups were not significantly heterogeneous (Fig. S3C).

The Kupffer cells are intrinsic hepatic macrophages vital in maintaining hepatic and immune homeostasis. In addition, they are an essential cell type that should be included in liver fibrosis. Cluster analysis identified nine distinct clusters of Kupffer cells (Fig. S3D). Interestingly, the proportion of each cluster in the total number of Kupffer cells between the two groups was not significantly different (Fig. S3E). Moreover, differential gene expression analysis revealed no noteworthy heterogeneity between the control and oxytocin groups (Fig. S3F). Although OXTRs were also expressed by Kupffer cells in human and mouse livers (Fig. S3G), oxytocin did not induce changes in OXTRs in the Kupffer cells in the CCl_4 liver fibrosis model (Fig. S3H). Thus, the findings suggested that Kupffer cells might not be significant in liver fibrosis reversal by oxytocin.

Although macrophages are key in inflammation and tissue fibrosis development,[11] single-cell sequencing results have ruled out several important potential target cells for oxytocin within the liver. However, the functional heterogeneity of macrophage subtypes *in vivo* and their multifaceted roles in fibrotic regression do not entirely elucidate the possible effects of oxytocin on macrophages.

In this study, we focused on mononuclear cell-derived macrophages. The cluster analysis of single-cell sequencing data identified eight distinct macrophage clusters in all liver specimens (clusters 1–8). Notably, cell cluster 2 displayed high APOE expression, whereas cell cluster 3 exhibited elevated Ly6C and CCR2 expression. In addition, cell cluster 4 demonstrated significant Mrcr1 (CD206) expression, and cell cluster 6 exhibited high MMP12 expression (Fig. 3B and Fig. S3I).

Previous research has heavily used Ly6C differential expression to identify distinct monocyte and macrophage populations with specific functions.[12] Ly6C differential expression is often used to accurately identify and characterize previously elusive macrophages associated with liver fibrosis recovery.[13] Specifically, this subset of macrophages is the primary population expressing MMPs during hepatic fibrosis regression, and their function is crucial for degrading tissue scarring.[14] Among the eight macrophage subgroups, clusters 1, 3, 5, and 7 highly expressed Ly6C. Consequently, we considered clusters 1, 3, 5, and 7 $Ly6C^{high}$ macrophage clusters and clusters 2, 4, 6, and 8 $Ly6C^{low}$ macrophage clusters (Fig. 3C). The analysis of Ly6C macrophage cluster cell numbers determined that the oxytocin group had an increased percentage of $Ly6C^{low}$ macrophage cluster cells compared with the control group. Conversely, the oxytocin group had a decreased percentage of $Ly6C^{high}$ macrophage cluster cells (Fig. 3D). The oxytocin group $Ly6C^{low}$ macrophage clusters had higher ApoE, KLF4, SOCS3, MMP9, and MMP12 expression than those in the control group, whereas COX-2 expression was significantly lower (Fig. 3E). These findings indicated that oxytocin might affect the relative distribution of Ly6C macrophage subpopulations.

Oxytocin drives $Ly6C^{high}$/$Ly6C^{low}$ macrophage phenotype switch

The above results were verified by examining the proportions of $Ly6C^{high}$ and $Ly6C^{low}$ macrophage subpopulations using flow cytometry in a CCl_4-induced hepatic fibrosis mouse model and a mouse model of BDL hepatic fibrosis. The results revealed significantly increased proportions of $Ly6C^{low}$ macrophage subpopulations in response to oxytocin (Fig. 3F). Immunofluorescence staining demonstrated variations in Ly6C expression within the mouse liver macrophages following oxytocin administration (Fig. 3G). *In vitro* experiments were conducted

revealed that Ly6C was highly expressed in the OXTR group. Scale bars: 50 μm. (D) Serum ALT and AST liver injury profiles of mice in each group. The degree of liver injury was higher in the $OXTR^{myel\text{-}KO}$ group than in the $OXTR^{myel\text{-}WT}$ group. (E) Western blotting results showed that fibrosis-related proteins ColIA1, α-SMA, and GFAP were highly expressed in the livers of mice in the $OXTR^{myel\text{-}KO}$ group compared with the $OXTR^{myel\text{-}WT}$ group. (F) Flow cytometry results showed that the percentage of liver $Ly6C^{high}$ macrophage subpopulation was higher in the $OXTR^{myel\text{-}KO}$ group than in the $OXTR^{myel\text{-}WT}$ group, whereas $Ly6C^{low}$ was lower in the $OXTR^{myel\text{-}KO}$ group than in the $OXTR^{myel\text{-}WT}$ group. (G) The relative mRNA expression levels of $Ly6C^{high/low}$ macrophage subpopulation-related genes *ACTA2*, *COLA1*, *Ly6C*, *MMP3*, *MMP9*, and *PDGFRB* in the livers of the two groups. (H) Relative mRNA expression levels of *Ly6C*, *CD86*, *MMP3*, *MMP9*, *MMP12*, *SOCS3*, and *TIMP1* in LPS-stimulated BMDM (from the $OXTR^{myel\text{-}KO}$ group and the $OXTR^{myel\text{-}WT}$ group) with or without oxytocin receptor after oxytocin stimulation. Statistical analyses were performed using a two-tailed unpaired *t* test or one-way ANOVA with Tukey's *post hoc* test. Error bars indicate SEM; $^{*}p$ <0.05, $^{**}p$ <0.01, $^{***}p$ <0.001, $^{****}p$ <0.0001. α-SMA, α-smooth muscle actin; ALT, alanine aminotransferase; AST, aspartate aminotransferase; BMDM, bone marrow-derived macrophage; CCl_4, carbon tetrachloride; GFAP, glial fibrillary acidic protein; KO, knockout; LPS, lipopolysaccharide; MMP3/9/12, matrix metalloproteinase 3/9/12; OXT, oxytocin; OXTR, oxytocin receptor; TMP1, tissue inhibitor of metalloproteinase 1; WT, wild-type.

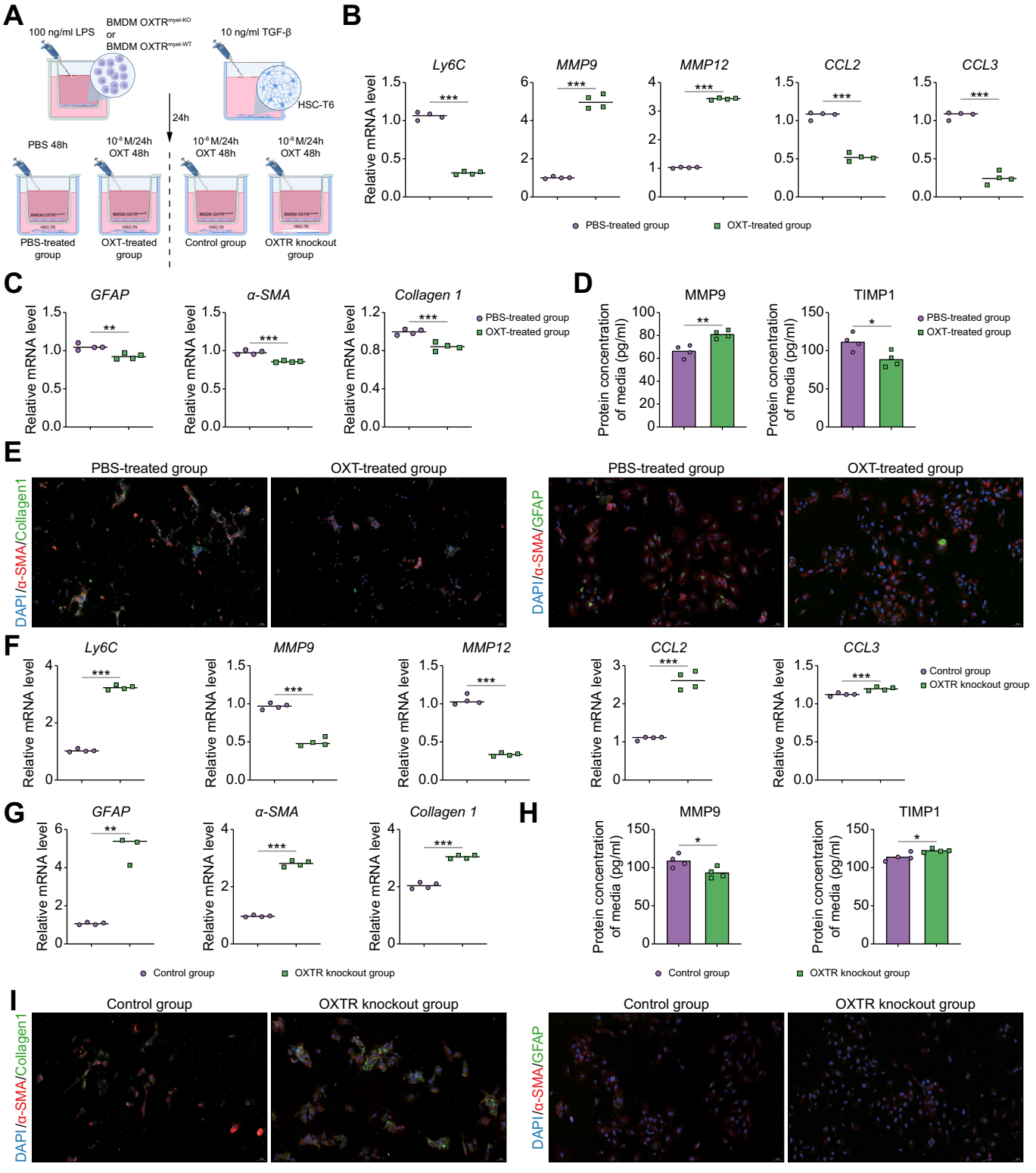

Fig. 5. The *in vitro* co-culture system verified that the Ly6C^{high}/Ly6C^{low} phenotypic shift affected HSC activation and secretion. (A) Schematic diagram of the *in vitro* co-culture system of LPS-stimulated BMDM and TGF-β-activated HSC. (B) For LPS-stimulated BMDM cells treated with PBS or OXT, the mRNA expression of Ly6C, CCL2, and CCL3 was decreased and the expression of mmp9 and mmp12 was elevated in the OXT-treated group. (C) After TGF-β-activated HSC cells were cultured in the co-culture system for 48 h, the expression of GFAP, a marker of HSC activation, was significantly lower in the oxytocin-treated group than in the PBS-treated group, and the expression of α-SMA and collagen 1, important components of fibrosis, was significantly lower than in the PBS group. (D) ELISA detected the expression of mmp9 and TIMP1 in the supernatant of cell culture medium in the co-culture system. The protein concentration of mmp9 in the supernatant of cell culture medium in the oxytocin-treated co-culture system was higher than that in the PBS-treated group, and TIMP1 was lower in the oxytocin-treated group than in the PBS-treated group. (E) Immunofluorescence results further showed that the expression of GFAP, a marker of HSC activation, was significantly lower in the oxytocin-treated group than in the PBS group, and the expression of α-SMA and collagen 1, an important component of fibrosis, was

using BMDMs induced to express a pro-inflammatory phenotype using interferon-γ (IFN-γ) and LPS. Oxytocin significantly reduced Ly6C expression in the pro-inflammatory BMDMs (Fig. 3H). In addition, CD86 (a pro-inflammatory macrophage marker) was downregulated, and TIMP1, MMP3, and MMP9 expressions were altered, suggesting a reversal of the pro-inflammatory phenotypic switch (Fig. 2I).

The above results were confirmed using THP-1-derived macrophages (Fig. 3J and Fig. S2G), which supported the observations made in the previous experiments, highlighting the consistency of the effect of oxytocin on macrophage subpopulations and inflammatory phenotypes. These findings enhanced the potential translational relevance of oxytocin-mediated modulation of macrophage function in human immune responses.

Oxytocin-driven Ly6C^{low} macrophage population promotes hepatic fibrosis regression

The role of recruitment-derived macrophages in the antihepatic fibrotic effects mediated by the oxytocin signaling system was investigated by breeding myeloid-derived cellular OXTR knockout mice. The ultrasound results (Fig. 4A) demonstrated that silencing the OXTR eliminated the antihepatic fibrotic effects of oxytocin. This result was supported by consistent results from the immunohistochemical and Western blotting analyses (Fig. 4B and E). The OXTR$^{myel\text{-}KO}$ mice had significantly higher serum ALT and AST levels than the control group (Fig. 4D). The immunofluorescence staining and flow cytometry results revealed that oxytocin did not affect Ly6C cell population redistribution in the OXTR$^{myel\text{-}KO}$ mice (Fig. 4C and F). Knocking down the OXTR increased the mRNA expression levels of ACTA2 (α-SMA), COLA1, Ly6C, and PDGFRB in the liver while reducing MMP3 and MMP9 expression levels (Fig. 4G). Furthermore, the OXTR deficiency meant that oxytocin could not reverse the LPS-induced upregulation of Ly6C and related inflammatory genes in the BMDMs from OXTR knockout mice (Fig. 4H). The sex dichotomy of the oxytocin reversal of hepatic fibrosis was examined using α-SMA and Sirius Red staining. The results demonstrated that sex did not affect the role of oxytocin in liver fibrosis (Fig. S2J).

The mechanism underlying the interactions between Ly6C^{low} macrophages and activated HSCs induced by oxytocin was elucidated by establishing an *in vitro* co-culture system using activated HSC-T6 cells and inflammatory BMDMs with or without oxytocin treatment (Fig. 5A). The oxytocin-treated inflammatory BMDMs had significantly decreased Ly6C, CCL2, and CCL3 expression and upregulated MMPs compared to the control group (Fig. 5B). Moreover, the activated HSC-T6 cells in the oxytocin group had reduced GFAP, α-SMA, and collagen 1 expression compared with the PBS-treated group (Fig. 5C and E). ELISA revealed altered solubility factor levels in the conditioned medium of the oxytocin group, including increased MMP9 and TIMP1 secretion (Fig. 5D). The role of oxytocin in promoting inflammatory factor secretion by BMDMs and its effect on restoring HSC activation was investigated using a targeted approach by selectively knocking out the OXTR in BMDMs. The results demonstrated that the *in vitro* promotion of BMDM secretion by oxytocin to reverse HSC activation was lost (Fig. 5F–I).

Oxytocin treatment drives the macrophage phenotype switch via NR4A1 activation

The molecular mechanism underlying the beneficial effects of the oxytocin signaling system in liver fibrosis was investigated by conducting Kyoto Encyclopedia of Genes and Genomes (KEGG) analysis on transcriptome data obtained from the oxytocin-treated liver fibrosis mice (Fig. 6A and B). We determined that the upregulation of NR4A1, a key regulator, was enriched in two critical inflammatory pathways. Previous studies reported that NR4A1 is crucial in Ly6C^{low} monocyte production and survival, and its overexpression alleviates fibrosis in multiple organs. Accordingly, we aimed to determine whether the oxytocin signaling system regulates macrophage phenotypic switching by influencing NR4A1 expression.

Our results demonstrated that exogenous oxytocin significantly increased NR4A1 expression in macrophages specifically within the cholestatic liver (Fig. 6C). Moreover, oxytocin promoted upregulated NR4A1 expression. It facilitated its translocation from the cytoplasm to the nucleus in BMDMs, suggesting a potential link between NR4A1 activation and oxytocin-induced switching of the Ly6C phenotype in macrophages (Fig. 6D). We observed that pro-inflammatory stimulation reduced BMDM NR4A1 expression by 50%. In contrast, oxytocin upregulated its expression to levels comparable with, or even higher than, those observed in unpolarized control cells (Fig. 6E). Conversely, knocking down the OXTR prevented this (Fig. 6F).

The importance of NR4A1 activation in the oxytocin-mediated phenotypic switch was investigated by specific silencing of NR4A1 expression in RAW264.7 cells (Fig. 6G). The results demonstrated that oxytocin treatment in the siControl group upregulated MRC1, MMP3, MMP9, and MMP12 while downregulating Ly6C and CD86. However, no similar effects were observed in the siNr4A1 group (Fig. 6H), highlighting the indispensability of NR4A1 activation for the oxytocin-mediated phenotypic switch.

Overall, these findings suggested that oxytocin drives the macrophage phenotype switch by activating NR4A1.

Regulatory mechanism of calcium-dependent NR4A1 by the oxytocin signaling system

Previous studies reported that the oxytocin signaling system is important in signal transduction by regulating myometrium and neuron calcium levels. However, how oxytocin signaling in

significantly lower in the PBS group. Scale bars: 100 μm. (F) The inhibitory effect of contraction on LPS-stimulated inflammation in BMDM disappeared after the contraction receptor was silenced. The expression of Ly6C, CCL2, and CCL3 was higher in the contraction receptor knockout group than in the control group, and the expression of mmp9 and mmp12 was reduced. (G) The expression of GFAP, α-SMA, and collagen 1 (an activation index of HSCs) was significantly higher in the OXTR knockout group than in the control group. (H) The protein concentration of mmp9 in the supernatant of the cell culture medium of the peptide receptor knockout group was lower than that of the control group, and TIMP1 was higher than that of the control group. (I) Immunofluorescence results showed that the expression of HSC activation markers GFAP, α-SMA, and collagen 1 was significantly higher in the OXTR knockout group than in the control group. Scale bars: 100 μm. Statistical analyses were performed using a two-tailed unpaired *t* test or one-way ANOVA with Tukey's *post hoc* test. Error bars indicate SEM; $^{*}p$ <0.05, $^{**}p$ <0.01, $^{***}p$ <0.001, $^{****}p$ <0.0001. α-SMA, α-smooth muscle actin; BMDM, bone marrow-derived macrophage; GFAP, glial fibrillary acidic protein; HSC, hepatic stellate cell; LPS, lipopolysaccharide; MMP9/12, matrix metalloproteinase 9/12; OXT, oxytocin; OXTR, oxytocin receptor; TGF-β, transforming growth factor β; TMP1, tissue inhibitor of metalloproteinase 1.

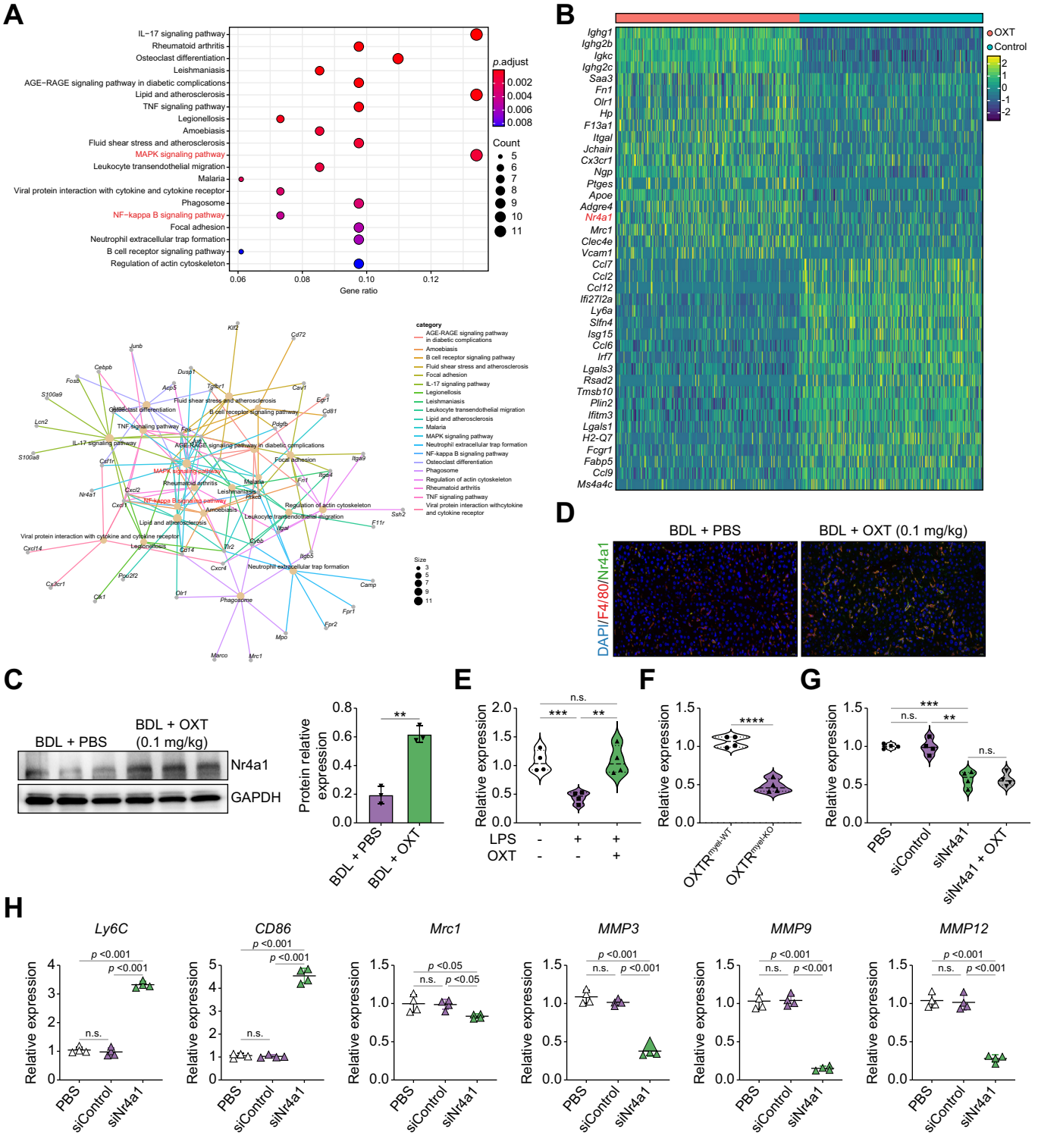

Fig. 6. OXT treatment drives the macrophage phenotype switch via Nr4A1 activation. (A) KEGG analysis was performed on transcriptome data from mice with liver fibrosis. (B) *Nr4A1* as a key regulatory gene of the inflammatory pathway was upregulated in the OXT-treated group. (C) Relative mRNA expression levels of Nr4A1 in BDL-induced fibrotic livers with or without OXT treatment. (D) Representative immunofluorescence staining of Nr4A1 and F4/80 in BDL-induced fibrotic livers with or without OXT treatment. The quantification of total Nr4a1 expression and % Nr4a1 expression in the cell nucleus was performed in five randomly selected fields per sample using ImageJ (n = 3 biologically independent samples per group). Scale bars: 100 μm. (E) Relative mRNA expression levels of Nr4A1 in BMDMs with or without LPS + IFN-γ stimulation and OXT treatment. (F) Relative mRNA expression levels of Nr4A1 in BMDMs with or without OXTR. (G) Relative mRNA expression levels of Nr4A1 in RAW264.7 cells without treatment (PBS), transfected with scrambled siCtr or siNr4a1. (H) Relative mRNA expression of *Ly6C*, *CD86*, *MRC1*, *MMP3*, *MMP9*, and *MMP12* in Nr4A1-knockdown RAW264.7 cells after OXT treatment. Statistical analyses were performed using a two-tailed unpaired *t* test or one-way ANOVA with Tukey's *post hoc* test. Error bars indicate SEM; **p* <0.05, ***p* <0.01, ****p* <0.001, *****p* <0.0001. BDL, bile duct ligation; BMDM, bone marrow-derived macrophage; IFN-γ, interferon-γ; KEGG, KEGG, Kyoto Encyclopedia of Genes and Genomes; KO, knockout; LPS, lipopolysaccharide; MMP3/9/12, matrix metalloproteinase 3/9/12; OXT, oxytocin; OXTR, oxytocin receptor; WT, wild-type.

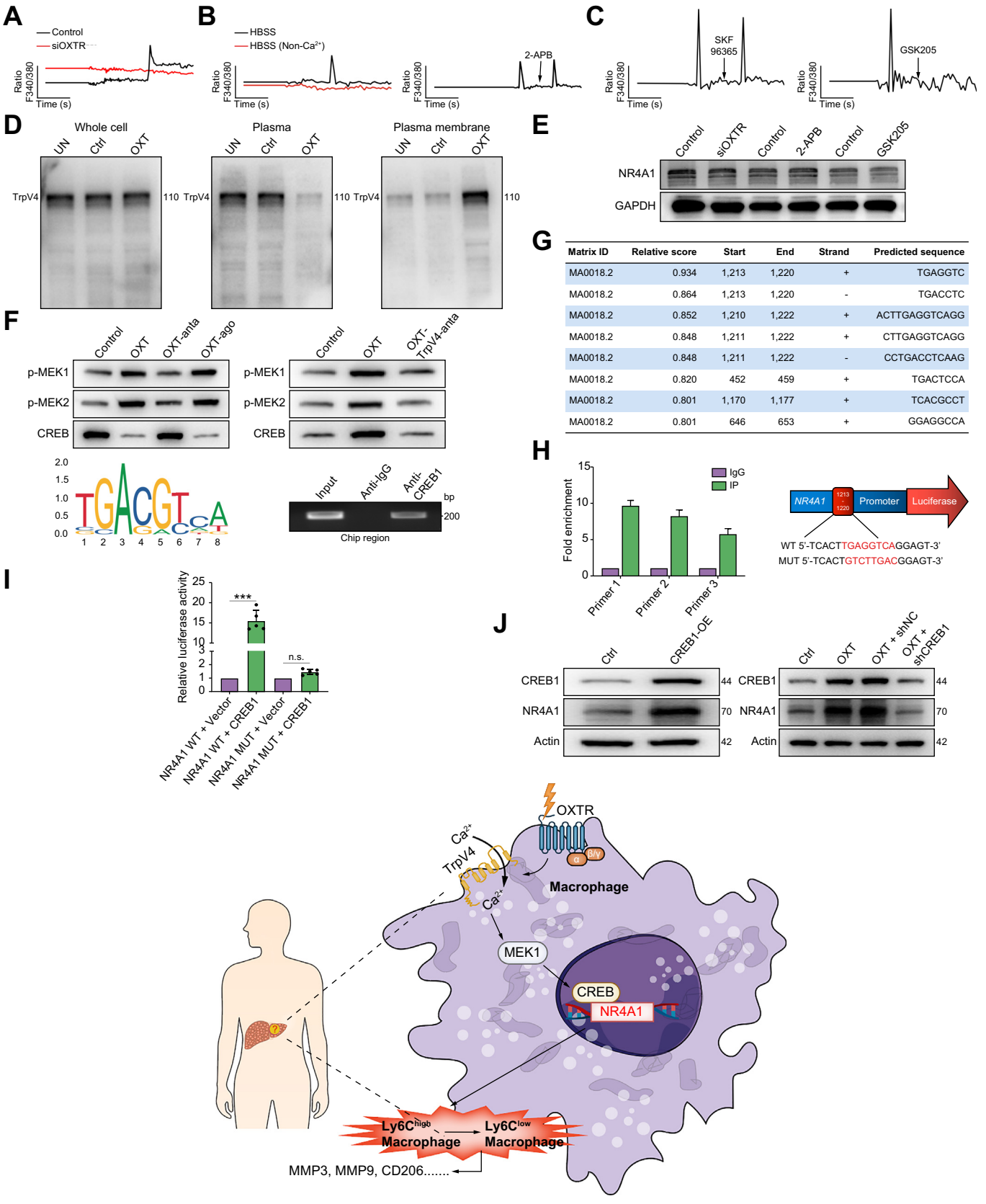

Fig. 7. Regulation mechanism of calcium-dependent Nr4A1 by OXT signaling system. (A) OXT-induced calcium influx was eliminated after silencing of OXTRs in BMDM. (B) The calcium influx induced by OXT disappeared after the extracellular calcium ion disappeared. After blocking the calcium channel of the endoplasmic reticulum, the calcium ion influx induced by OXT had no change. (C and D) OXT induced calcium influx by activating TRPV4 channels through specific inhibitors SKF96365 and GSK205. (E) Nr4A1 expression was reduced after silencing of OXT receptor and TRPV4 channels. (F) The activation of the OXT

macrophages functions remains unclear. Monitoring the BMDM intracellular calcium levels revealed that silencing the OXTR eliminated the calcium influx peak of the macrophages (Fig. 7A). Removing the extracellular calcium ions of macrophages and blocking the internal quality mesh calcium ion channel revealed that the calcium ion peak induced by the shrinking giyin signal system originated from calcium ion internal flow (Fig. 7B). Blocking specific calcium channels with the TRPV2 and TRPV4 calcium channel inhibitors SKF96365 and GSK205 revealed that the oxytocin signaling system induced calcium influx through TRPV4 calcium channels in the macrophage membrane (Fig. 7C and D). The relationship between calcium ions and NR4A1 was investigated by silencing OXTRs and specific calcium channels and reducing intracellular calcium levels, which decreased NR4A1 protein in the macrophages, indicating that the oxytocin signaling system affected the NR4A1 expression level by regulating the calcium ion influx (Fig. 7E). The oxytocin signaling system activation and calcium ion influx activated the classic inflammatory pathway MEK1/2 in the liver and upregulated the transcription factor CREB (Fig. 7F). Furthermore, the dual-luciferase reporter assay demonstrated that CREB bound to the *NR4A1* 1213–1200 promoter region (Fig. 7G). We also constructed luciferase reporter vectors containing WT or mutant CREB-binding sequences, and the results demonstrated that mutations in the binding site destroyed the ability of CREB to promote NR4A1 expression (Fig. 7H–J). In summary, the oxytocin signaling system activated the MAPK pathway through calcium influx and promoted CREB transcription factor binding to the NR4A1 promoter region, thus conducting the function of the NR4A1 phenotypic switch.

Discussion

Liver fibrosis is characterized by a self-injury repair process influenced by various injurious factors and frequently progresses to severe liver dysfunction caused by an imbalanced repair mechanism.[15] The current therapeutic approaches for fibrosis primarily involve addressing the injurious factors and targeting the fibrotic process.[16] Addressing the injurious factors typically involves reducing liver injury etiologies, such as clinical interventions for viral hepatitis. However, effective interventions for the underlying liver fibrotic pathology are limited and insufficient.[17] Thus, investigating efficacious and secure liver fibrosis interventions represents a crucial research focus in liver disease.

Oxytocin is a pharmaceutical agent with a long history of safe usage in obstetrics and gynecology that has gained significant attention and potential applications beyond its traditional scope. Previously, we determined that oxytocin inhibited mast cell degranulation through the calcium ion–nitric oxide synthase pathway to exert analgesic effects,[18] reduce vincristine-induced nerve damage,[19] reduce dextran sulfate sodium-induced colitis by regulating dendritic cell immune tolerance,[20] and reduce intestinal inflammation by regulating macrophage polarization.[21]

We recently shifted our oxytocin research focus to the liver, an important organ, and simultaneously reported OXTR expression in the liver for the first time. In the present study, a reliable liver fibrosis model and single-cell sequencing technology enabled the discovery of the therapeutic effect of oxytocin on liver fibrosis by targeting recruitment-derived Ly6C^{high} macrophages and promoting their conversion to the Ly6C^{low} inverse liver fibrosis phenotype. The resulting Ly6C^{low} macrophage phenotype reversed HSC activation and attenuated hepatic fibrosis progression by decreasing pro-inflammatory cytokine and chemokine expression and increasing scar-degrading gene expression (MMPs and TIMP1).

Furthermore, our data revealed the limitations of classifying macrophage populations in the *in vivo* environment into the widely used but restrictive M1/M2 paradigm. The alternative activation effect of oxytocin on M2 macrophages contradicts the common knowledge that M2 macrophages promote liver fibrosis.[22] The traditional phenotype classification of macrophage activation and alternative activation can no longer explain the alleviation effect of oxytocin on liver fibrosis in our study. Single-cell sequencing yields more dimensional information about cellular transformation. Compared with the traditional M1/M2 macrophage phenotype switch, which indirectly affects liver fibrosis through inflammation, oxytocin regulation of macrophage Ly6C^{high}/Ly6C^{low} subgroups more intuitively demonstrates the dual role of macrophages in liver fibrosis progression and alleviation. During fibrosis progression, macrophage secretion of CCL2 recruits immature monocyte-derived Ly6C^{high} macrophages to the liver and produces chemokines to induce HSC activation.[23] During liver fibrosis regression, Ly6C^{low} macrophages reduce inflammatory factor production[24] and secrete MMPs to promote collagenolytic activity and ECM phagocytosis by macrophages.[25] Oxytocin regulation of the macrophage phenotypes suggests that oxytocin has different liver fibrosis progression/alleviation pathways.

Furthermore, we elucidated the signaling pathway from OXTR activation to the phenotypic switch by NR4A1 activation.[26] Previous studies of calcium signaling following oxytocin signaling system activation focused on the nervous system,[27] but little was known about the transcriptional cascades initiated by elevated cytoplasmic calcium ion levels. Our study demonstrated that calcium influx induced by OXTR activation activated NR4A1, a key orphan nuclear receptor, to function as a phenotypic switch. Furthermore, we identified CREB as a targeted modulator of the calcium ion pathway to stimulate NR4A1 expression in cells and suggested that CREB is required for NR4A1 expression and phenotypic switching.

In summary, we described the sequential steps of oxytocin-induced macrophage phenotype switching and demonstrated that oxytocin signaling system activation is a promising strategy to alleviate liver fibrosis and follow up the detailed mechanisms by which it exerts its effects. The potential applications of oxytocin and its analogues as traditional drugs for clinical application in treating liver fibrosis require further study.

signaling system and the influx of calcium ions led to the activation of the classic inflammatory pathway MEK1/2 in the liver and the upregulation of the transcription factor CREB. (G–I) Dual-luciferase reporter assay showed that CREB bound to the Nr4A1 1213–1200 promoter region. ChIP analysis of CREB1 binding to the Nr4A1 promoter. The input and IgG served as positive and negative controls, respectively. Cells were transfected with Nr4A1-WT or Nr4A1-MUT promoter constructs, and luciferase activity was analyzed after transfection. (J) Western blotting results further proved the role of CREB as an important transcription factor in the regulation of Nr4A1 expression. Statistical analyses were performed using a two-tailed unpaired *t* test or one-way ANOVA with Tukey's *post hoc* test. Error bars indicate SEM; **p* <0.05, ***p* <0.01, ****p* <0.001, *****p* <0.0001. 2-APB, 2-aminoethyl diphenylborinate; BMDM, bone marrow-derived macrophage; ChIP, chromatin immunoprecipitation; HBSS, Hank's balanced salt solution; IP, immunoprecipitation; MMP3/9/12, matrix metalloproteinase 3/9/12; MUT, mutation; OXT, oxytocin; OXTR, oxytocin receptor; UN, untreated; WT, wild-type.

Abbreviations

α-SMA, α-smooth muscle actin; ALT, alanine aminotransferase; AST, aspartate aminotransferase; BDL, bile duct ligation; BMDM, bone marrow-derived macrophage; CCl_4, carbon tetrachloride; cDNA, complementary DNA; ChIP, chromatin immunoprecipitation; co-IP, co-immunoprecipitation; ECM, extracellular matrix; GFAP, glial fibrillary acidic protein; HSC, hepatic stellate cell; IFN-γ, interferon-γ; KEGG, Kyoto Encyclopedia of Genes and Genomes; LPS, lipopolysaccharide; MMP3/9/12, matrix metalloproteinase 3/9/12; OXT, oxytocin; OXTR, oxytocin receptor; qRT-PCR, quantitative real-time PCR; TGF-β, transforming growth factor-beta; TMP1, tissue inhibitor of metalloproteinase 1; UMAP, uniform manifold approximation and projection; WT, wild-type.

Financial support

This work was supported by the Second Hospital of Shandong University Cultivation Funding (No. 2022YP45).

Conflicts of interest

The authors declare that there is no conflict of interest regarding the publication of this article.

Please refer to the accompanying ICMJE disclosure forms for further details.

Authors' contributions

Conceived the hypothesis: XYZ, XSL, WW, BJ. Performed the experiments: XYZ, HZ, ZJX, MKL, GD, ZCJ. Designed and interpreted the results: XYZ, ZJX, HXZ, DL, DDD. Wrote the manuscript: XY, HZ, BJ. Supervised the study, JXL, WW. Read and approved the final version of the manuscript: all authors.

Data availability statement

All the data needed to evaluate the conclusions of the study are provided within the paper. Additional data related to this study can be requested from the authors.

Supplementary data

Supplementary data to this article can be found online at https://doi.org/10.1016/j.jhepr.2024.101032.

References

Author names in bold designate shared co-first authorship

[1] Carcea I, Caraballo NL, Marlin BJ, et al. Oxytocin neurons enable social transmission of maternal behaviour. Nature 2021;596:553–557.
[2] Sikich L, Kolevzon A, King BH, et al. Intranasal oxytocin in children and adolescents with autism spectrum disorder. N Engl J Med 2021;385:1462–1473.
[3] Raut SB, Marathe PA, van Eijk L, et al. Diverse therapeutic developments for post-traumatic stress disorder (PTSD) indicate common mechanisms of memory modulation. Pharmacol Ther 2022;239:108195.
[4] Li XH, Matsuura T, Xue M, et al. Oxytocin in the anterior cingulate cortex attenuates neuropathic pain and emotional anxiety by inhibiting presynaptic long-term potentiation. Cell Rep 2021;36:109411.
[5] Pan S, Yin K, Tang Z, et al. Stimulation of hypothalamic oxytocin neurons suppresses colorectal cancer progression in mice. Elife 2021;10.
[6] Carter CS, Kenkel WM, MacLean EL, et al. Is oxytocin "nature's medicine". Pharmacol Rev 2020;72:829–861.
[7] Luo D, Jin B, Zhai X, et al. Oxytocin promotes hepatic regeneration in elderly mice. iScience 2021;24:102125.
[8] Zhai X, Wang W, Dou D, et al. A novel technique to prepare a single cell suspension of isolated quiescent human hepatic stellate cells. Sci Rep 2019;9:12757.
[9] Zhai X, Xia Z, Du G, et al. LRP1B suppresses HCC progression through the NCSTN/PI3K/AKT signaling axis and affects doxorubicin resistance. Genes Dis 2023;10:2082–2096.
[10] Zhai X, Wang W, Ma Y, et al. Serum KIAA1199 is an advanced-stage prognostic biomarker and metastatic oncogene in cholangiocarcinoma. Aging (Albany NY) 2020;12:23761–23777.
[11] Kisseleva T, Brenner D. Molecular and cellular mechanisms of liver fibrosis and its regression. Nat Rev Gastroenterol Hepatol 2021;18:151–166.
[12] Wynn TA, Barron L. Macrophages: master regulators of inflammation and fibrosis. Semin Liver Dis 2010;30:245–257.
[13] Tyralla K, Adamczak M, Benz K, et al. High-dose enalapril treatment reverses myocardial fibrosis in experimental uremic cardiomyopathy. PLoS One 2011;6:e15287.
[14] Hu M, Wang Y, Liu Z, et al. Hepatic macrophages act as a central hub for relaxin-mediated alleviation of liver fibrosis. Nat Nanotechnol 2021;16:466–477.
[15] Roehlen N, Crouchet E, Baumert TF. Liver fibrosis: mechanistic concepts and therapeutic perspectives. Cells 2020;9:875.
[16] Gish RG, Wong RJ, Di Tanna GL, et al. Association between hepatitis delta virus with liver morbidity and mortality: a systematic literature review and meta-analysis. Hepatology 2023. https://doi.org/10.1097/HEP.0000000000000642.
[17] De Blasio MJ, Ohlstein EH, Ritchie RH. Therapeutic targets of fibrosis: translational advances and current challenges. Br J Pharmacol 2023;180:2839–2845.
[18] Gong L, Li J, Tang Y, et al. The antinociception of oxytocin on colonic hypersensitivity in rats was mediated by inhibition of mast cell degranulation via Ca^{2+}-NOS pathway. Sci Rep 2016;6:31452.
[19] Zhu J, Li Y, Liang J, et al. The neuroprotective effect of oxytocin on vincristine-induced neurotoxicity in mice. Toxicol Lett 2021;340:67–76.
[20] Dou D, Liang J, Zhai X, et al. Oxytocin signalling in dendritic cells regulates immune tolerance in the intestine and alleviates DSS-induced colitis. Clin Sci (Lond) 2021;135:597–611.
[21] Shi Y, Li S, Zhang H, et al. The effect of macrophage polarization on the expression of the oxytocin signalling system in enteric neurons. J Neuroinflammation 2021;18:261.
[22] Ma PF, Gao CC, Yi J, et al. Cytotherapy with M1-polarized macrophages ameliorates liver fibrosis by modulating immune microenvironment in mice. J Hepatol 2017;67:770–779.
[23] Baeck C, Wehr A, Karlmark KR, et al. Pharmacological inhibition of the chemokine CCL2 (MCP-1) diminishes liver macrophage infiltration and steatohepatitis in chronic hepatic injury. Gut 2012;61:416–426.
[24] Ramachandran P, Pellicoro A, Vernon MA, et al. Differential Ly-6C expression identifies the recruited macrophage phenotype, which orchestrates the regression of murine liver fibrosis. Proc Natl Acad Sci U S A 2012;109:E3186–E3195.
[25] Shi CX, Wang Y, Jiao FZ, et al. Epigenetic regulation of hepatic stellate cell activation and macrophage in chronic liver inflammation. Front Physiol 2021;12:683526.
[26] Monga M, Campbell DF, Sanborn BM. Oxytocin-stimulated capacitative calcium entry in human myometrial cells. Am J Obstet Gynecol 1999;181:424–429.
[27] Armstrong WE, Foehring RC, Kirchner MK, et al. Electrophysiological properties of identified oxytocin and vasopressin neurones. J Neuroendocrinol 2019;31:e12666.